IEEE Access
Multidisciplinary | Rapid Review | Open Access Journal

Received November 8, 2021, accepted December 9, 2021, date of publication December 20, 2021,
date of current version December 30, 2021.

Digital Object Identifier 10.1109/ACCESS.2021.3136550

Lumped-Capacitive Modeling and Sensing Characteristics of an Electrolyte-Gated FET Biosensor for the Detection of the Peanut Allergen

DONGHOON KIM[1], WONYEONG CHOI[1], SEONGHWAN SHIN[1], JIWON PARK[1], KIHYUN KIM[2], (Member, IEEE), BO JIN[1,3], AND JEONG-SOO LEE[1], (Senior Member, IEEE)

[1]Department of Electrical Engineering, Pohang University of Science and Technology (POSTECH), Pohang 37673, Republic of Korea
[2]Division of Electronics Engineering and Future Semiconductor Convergence Technology Research Center, Jeonbuk National University, Jeonju 54896, Republic of Korea
[3]Research and Development Department, Innovative General Electronic Sensor Technology co., ltd. (IGEST), Pohang 37673, Republic of Korea

Corresponding authors: Jeong-Soo Lee (ljs6951@postech.ac.kr) and Bo Jin (jinshengzhi1986@sina.com)

This work was supported in part by the Food, Agriculture, Forestry, and Fisheries (Institute of Planning and Evaluation for Technology, IPET) through the Animal Disease Management Technology Development Program, which is funded by the Ministry of Agriculture, Food, and Rural Affairs (MAFRA) under Grant 120091-02-1-CG000; and in part by the Ministry of Science and ICT (MSIT), South Korea, through the "Nanomaterial Technology Development Program," supervised by the National Research Foundation of Korea (NRF) under Grant 2009-0082580.

ABSTRACT Si-based electrolyte-gated transistors (EGTs) have been investigated to achieve high sensitivity and a low detection limit (LOD). Here, a lumped-capacitive model was applied to analyze the influence of receptor–target conjugates on the sensing performance. The voltage-related sensitivity is mainly determined by the effective dipole potential ($V_{DP,EFF}$), the effective capacitance of the functionalization layer ($C_{FN,EFF}$), and the total charge density in the channel (Q_S) related to the operating regime. In an n-type EGT, the sensitivity is enhanced as the device is operated in the subthreshold regime with a positive $V_{DP,EFF}$ and a small $C_{FN,EFF}$. The influence of the $V_{DP,EFF}$ and $C_{FN,EFF}$ was experimentally evaluated by detecting the peanut allergen (PA) using the fabricated n-type Si-EGTs. A higher sensitivity and a lower LOD could be achieved in the subthreshold regimes than in the linear regime. These results suggest that the proposed model is very useful to optimize the sensing characteristics of Si-based EGT for biosensing applications.

INDEX TERMS Capacitance, dipole moment, electrolyte-gated transistor, limit of detection, peanut allergen, silicon nanonet.

I. INTRODUCTION

Ion-sensitive field-effect transistors (ISFETs) have been investigated as promising diagnostic platforms for highly sensitive label-free biosensing [1]–[3]. Si-based, carbon-based, and organic ISFETs have been demonstrated to detect pH, DNA, proteins, and other biomolecules [4]–[9]. Owing to advances in fabrication technology, nanostructures have been extensively adopted as a channel layer to enhance the sensitivity and limit of detection (LOD) [10], [11]. In particular, Si-nanowires and organic/inorganic nanomaterial have proven to be capable of realizing highly sensitive responses with low power consumption [4]–[7]. However, a small channel area hosting a few bio-receptors requires more elaborate functionalization and the use of an external reference electrode, which could be significant hurdles in the commercialization of ISFETs.

Recently, electrolyte-gated transistors (EGTs) have been developed to detect various biomolecules and diagnose infectious diseases [9], [12]–[15]. A substantial advantage of EGT stems from the use of a large area of the gate electrode as the functionalized surface to ensure a high probability of receptor–target binding. The transfer ratio of the gate voltage to the channel potential is mainly determined from the capacitances at the gate/electrolyte, functionalized receptor/electrolyte, electrolyte/oxide interfaces, and the gate insulator [12], [13]. In addition to the capacitances, the receptor–target conjugate on the gate electrode induces a

The associate editor coordinating the review of this manuscript and approving it for publication was Norbert Herencsar.

surface dipole that can change the work function (ϕ_m) of the underlying material [14], [15].

To date, most EGTs have been fabricated and analyzed using conducting polymer films as their channel materials. Even though significant progress has been made in organic EGTs, these devices suffer from deformation and reliability issues compared to Si-based ISFET technology [16], [17].

Here, Si-nanonet (SiNN) EGTs were fabricated and characterized to achieve high sensitivity and low LOD values. A lumped-capacitive model was established to analyze the effects of receptor–target conjugates on the sensing performance. The sensitivity is significantly dependent on the surface dipoles, capacitance, and operation regime. Experiments were conducted on the detection of the peanut allergen (PA) to confirm the validity of the model and to extract the relevant dipole and capacitance components.

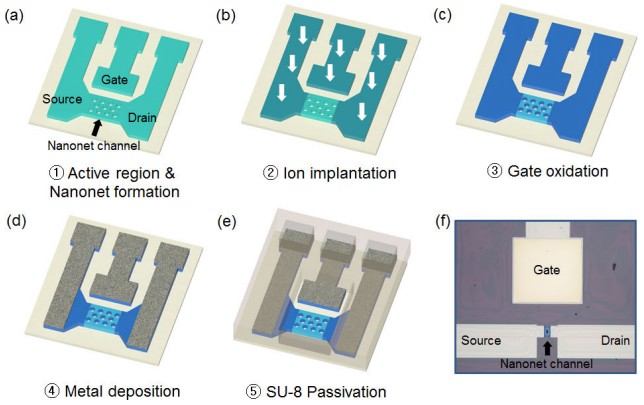

FIGURE 1. (a)–(e) Fabrication process flow of EGT and (f) optical image of fabricated EGT.

II. MATERIALS AND METHODS

A. DEVICE FABRICATION

SiNN EGTs were fabricated on an 8-inch silicon-on-insulator (SOI) wafer (boron-doped, ∼10 Ω·cm) with a 100 nm top-Si layer and a 400 nm buried oxide (BOX) layer using a top-down technique. Fig. 1 shows a schematic of the fabrication process flow of the SiNN EGTs. The active regions including the source, drain, and channel regions were formed using conventional photolithography and an inductively coupled plasma reactive ion etching (ICP-RIE) process. Then, As ions with a dose of $2 \times 10^{15}/\text{cm}^2$ were implanted into the source and drain regions, followed by rapid thermal annealing (RTA) at 1000 °C for 20 s. Next, a 5-nm-thin SiO_2 gate oxide was thermally grown using a wet oxidation process. Then, a 50/500 nm Ti/Ag layer was deposited using an e-beam evaporator and patterned using a conventional lift-off process to form contact pads, a gate electrode, and transmission lines. Finally, an SU-8 passivation layer was formed, except for at the channel, contact pads, and gate electrode regions.

Fig. 1(f) shows an optical image of the fabricated SiNN EGT in which the areas of the gate electrode and the channel are $\sim 300 \times 300\ \mu\text{m}^2$ and $\sim 10 \times 10\ \mu\text{m}^2$, respectively.

B. DEVICE FUNCTIONALIZATION

Thermal stable-soluble proteins (TSSPs) including Ara h1-h3 were used as the PA samples [18]. First, 1 g of roasted peanuts were finely ground and mixed with 10 mL carbonate buffer (0.1 M, pH 9.6). After being placed in boiling water for 15 min, the mixture was cooled to room temperature, followed by centrifugation at 3000 rpm at 4 °C for 15 min. The supernatant containing TSSP was filtered through Whatman No. 1 filter paper and dialyzed in phosphate-buffered saline (PBS) twice daily for 3 days.

The IgG monoclonal antibody (Mab) was developed through cell fusion and cell cloning using TSSPs as an immunogen. The Mab was treated with papain to obtain a fragment antibody binding (Fab), a binding site for an antigen on the Mab. After purification using a protein G column, PA antibodies that could selectively detect PA were successfully created.

A series of chemical treatments for PA antibody immobilization were simultaneously performed on the gate electrode and channel surface. First, the EGT devices were cleaned with ethanol and distilled water (DIW), followed by UV–ozone treatment for 1.5 min. Next, the devices were exposed to vaporized 3-aminopropyltriethoxysilane (APTES) for 1 min at 50 °C to form an amine group ($-NH_2$) on the surface of the gate electrode and the channel. Then, the amine-functionalized device was dipped in a 2.5% glutaraldehyde (GA) solution (1 × PBS) for 90 min to generate an aldehyde-terminated surface ($-CHO$). Finally, a 200 μg/mL PA antibody solution was dropped onto the devices and incubated under humid conditions for 1 h in a homemade reaction chamber.

To visualize and compare the density of functionalization on the gate electrode and the channel, gold nanoparticle (AuNP)-conjugated targets were monitored using scanning electron microscopy (SEM) images. Due to the limitation of conjugation of PA and AuNPs, streptavidin was used as a receptor and biotin with AuNPs was used as a target. The APTES and GA treatments before antibody immobilization were the same as those used for PA detection. Streptavidin (1 mg/mL) was reacted for 2 h, and biotin conjugated with AuNPs with a diameter of 10 nm was treated for 2 h.

C. ELECTRICAL MEASUREMENT

The electrical performance of the fabricated SiNN EGTs was characterized using a semiconductor parameter analyzer (Keithley 4200SCS, USA) at room temperature.

The drain current (I_D) was measured while the gate voltage (V_G) was swept from 0 V to 0.8 V to obtain a transfer curve (I_D vs. V_G). The drain (V_D) and source (V_S) voltages were always connected to constant voltages of 0.1 V and 0 V, respectively. The sensing responses were analyzed using transfer curves with various PA concentrations in the range of 10 pg/mL–1 mg/mL. A fixed volume of 20 μL and an incubation time of 20 min were used for PA binding to the

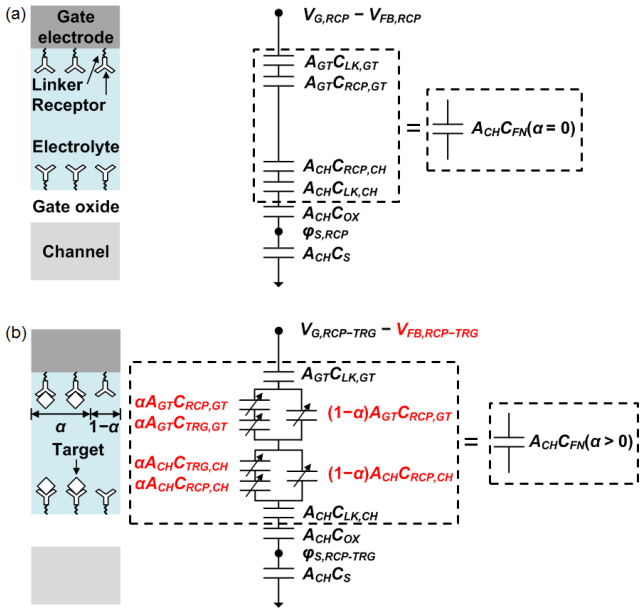

FIGURE 2. Schematic and equivalent circuit of EGT (a) after receptor immobilization and (b) after receptor–target binding.

antibody. After rinsing with deionized (DI) water, the devices were characterized in 0.01 × PBS solution.

III. RESULTS

A. ANALYTICAL MODELING

Understanding the detection mechanism related to the device's parameters is essential for improving the sensing response. The gate voltage and the threshold voltage in the FET operation are generally given by

$$V_G = V_{FB} + \varphi_S - \frac{Q_S(\varphi_S)}{C_{OX}} = V_{FB} + \varphi_S + \frac{1}{C_{OX}} \cdot \int_0^{\varphi_S} C_S d\varphi_S \quad (1)$$

$$V_{TH} = V_{FB} + 2\varphi_B - \frac{Q_S(2\varphi_B)}{C_{OX}} \quad (2)$$

where V_G is the gate voltage, V_{FB} is the flatband voltage, φ_S is the surface potential, Q_S is the area density of the total charges in the channel, C_{OX} is the capacitance per unit area of the gate oxide, C_S is the capacitance per unit area of the channel, V_{TH} is the threshold voltage, and φ_B is the difference between the Fermi potential and the intrinsic potential. Q_S is the sum of the depletion charge (Q_D) and inversion charge (Q_I) [19], [20].

The voltage-related sensitivity (S_V) is defined as the voltage difference before and after the binding event at a fixed I_D value, given by [21]

$$S_V = V_{G,RCP} - V_{G,RCP-TRG} \quad (3)$$

where $V_{G,RCP}$ and $V_{G,RCP-TRG}$ are the gate voltages at a specific I_D after receptor immobilization and the binding events, respectively.

Fig. 2 shows an equivalent circuit model for the sensing device. The functionalized layer consists of three different

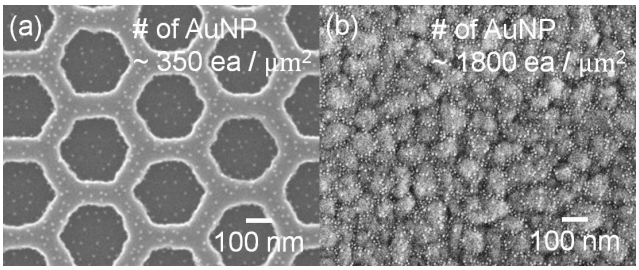

FIGURE 3. SEM images of AuNPs (diameter: 10 nm) on (a) the SiNN channel and (b) the gate electrode with the same functionalization.

capacitances (per unit area): the capacitance of the linker composed of APTES and GA (C_{LK}), the capacitance of the receptor (C_{RCP}), and the capacitance of the target (C_{TRG}). The binding factor α is defined as the ratio of the receptor sites bound with the target molecules to the total receptor sites ($0 \leq \alpha \leq 1$). The case after receptor immobilization is represented as $\alpha = 0$. α is generally expressed by a logistic Hill equation for binding analysis [22], [23]:

$$\alpha = \frac{N_{RCP-TRG}}{N_{RCP}} = \frac{[TRG]^n}{(K + [TRG]^n)} \quad (4)$$

where $N_{RCP-TRG}$ is the density of receptor–target conjugates, N_{RCP} is the density of total immobilized receptors, $[TRG]$ is the concentration of the target in the electrolyte, K is related to the dissociation constant of the receptor–target reaction, and n is a slope factor that indicates the cooperativity of target binding. The condition of $n < 1$ indicates a negative cooperativity, in which the first target bound on the receptor limits the second target approaching the other unreacted receptor [22], [23].

After introducing the receptor and/or the receptor–target conjugates, the surface can be electrically modeled using the dipole moment and coupled capacitance, as shown in Fig. 2(b) [12]–[15]. On the gate electrode and channel surface, the dipole moment generates the dipole potential (V_{DP}) as follows [14], [15]:

$$V_{DP} = \frac{N_{RCP-TRG} \cdot P_{DP}}{\varepsilon_{DP}} = \frac{\alpha \cdot N_{RCP} \cdot P_{DP}}{\varepsilon_{DP}} \quad (5)$$

where P_{DP} is the perpendicular component of the dipole moment, and ε_{DP} is the permittivity of the dipole layer. Depending on the type of receptor and target, P_{DP} has either a positive or negative value. In addition, V_{DP} is linearly proportional to $N_{RCP-TRG}$. Assuming that the same α both on the gate electrode and the channel, a higher N_{RCP} induces a larger V_{DP}. The effective dipole potential, $V_{DP,EFF}$, is given by

$$V_{DP,EFF} = V_{DP,GT} + V_{DP,CH} \quad (6)$$

where $V_{DP,GT}$ and $V_{DP,CH}$ are the dipole potentials at the gate electrode and channel, respectively. Both dipoles on the gate electrode and the channel have opposite polarity owing to the opposite direction of functionalization.

To analyze the effect of $V_{DP,GT}$ and $V_{DP,CH}$ on $V_{DP,EFF}$, SEM images of AuNPs on the gate electrode and the channel with the same functionalization are compared in Fig. 3.

Most of AuNPs were placed along the grain boundary of the gate electrode. The density of AuNPs on the gate electrode was 5–10 times larger than that on the channel. A larger density of the AuNPs implies a higher $N_{RCP-TRG}$ and N_{RCP}, followed by a higher V_{DP} according to (5). Thus, $V_{DP,GT}$ is the dominant factor affecting $V_{DP,EFF}$ for the fabricated devices.

$$V_{DP,EFF} \cong V_{DP,GT} \tag{7}$$

A positive $V_{DP,EFF}$ implies that the net electric field of the dipole layers is formed toward the gate electrode. To maintain the potential of the channel for the same I_D, a positive $V_{DP,EFF}$ should be eliminated by decreasing V_G, followed by a decrease in V_{FB} [14], [15]. Thus, $V_{DP,EFF}$ can directly affect V_{FB}, resulting in a shift of the transfer curve laterally according to (1). This equation is denoted as

$$V_{DP,EFF} = V_{FB,RCP} - V_{FB,RCP-TRG} \tag{8}$$

where $V_{FB,RCP}$ and $V_{FB,RCP-TRG}$ are the flat-band voltages after receptor immobilization and after receptor–target binding, respectively.

The receptor–target conjugate can be expressed as a series of combinations of C_{RCP} and C_{TRG}. The capacitance of the unbounded receptor can be denoted as $(1-\alpha)AC_{RCP}$, where A is the surface area. Then, the overall capacitance of the functionalization layer (C_{FN}), including all capacitances from the oxide surface to the gate electrode, can be expressed as follows:

$$C_{FN} = \left[\frac{1}{C_{LK,CH}} + \frac{A_{CH}}{A_{GT} \cdot C_{LK,GT}} + \frac{1}{\frac{\alpha}{\frac{1}{C_{RCP,CH}} + \frac{1}{C_{TRG,CH}}} + (1-\alpha) \cdot C_{RCP,CH}} + \frac{A_{CH}}{\frac{\alpha \cdot A_{GT}}{\frac{1}{C_{RCP,GT}} + \frac{1}{C_{TRG,GT}}} + (1-\alpha) \cdot A_{GT} \cdot C_{RCP,GT}} \right]^{-1} \tag{9}$$

where $C_{RCP,GT}$ and $C_{RCP,CH}$ are the receptor capacitances per unit area at the gate electrode and the channel, respectively; $C_{TRG,GT}$ and $C_{TRG,CH}$ are the target capacitances per unit area at the gate electrode and the channel, respectively; and A_{GT} and A_{CH} are the surface areas of the gate electrode and channel, respectively.

The relationship between V_G and φ_S after receptor immobilization and after receptor–target binding is given below [24]:

$$\frac{dV_{G,RCP}}{d\varphi_{S,RCP}} = 1 + C_S \left[\frac{1}{C_{OX}} + \frac{1}{C_{FN}\ (\alpha = 0)} \right] \tag{10}$$

$$\frac{dV_{G,RCP-TRG}}{d\varphi_{S,RCP-TRG}} = 1 + C_S \left[\frac{1}{C_{OX}} + \frac{1}{C_{FN}\ (\alpha > 0)} \right] \tag{11}$$

where $\varphi_{S,RCP}$ and $\varphi_{S,RCP-TRG}$ are the surface potentials after receptor immobilization and after target binding, respectively, and C_S is the channel capacitance per unit area.

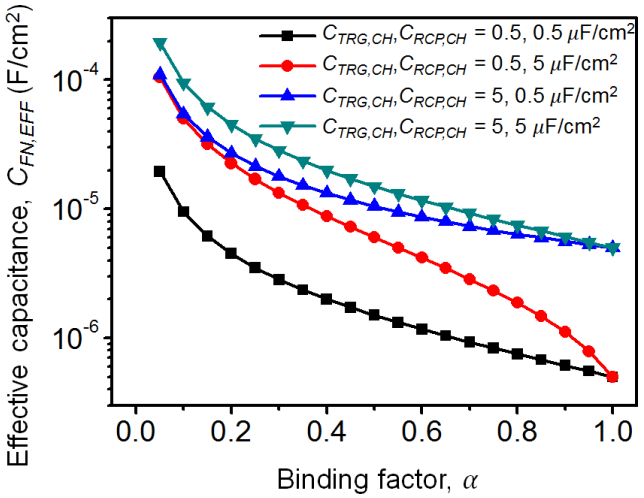

FIGURE 4. Dependence of $C_{FN,EFF}$ as a function of α with different $C_{TRG,CH}$ and $C_{RCP,CH}$ values.

Before and after the binding event, V_G can be rewritten by integrating (10) and (11) and by adding V_{FB}, as follows:

$$V_{G,RCP} = V_{FB,RCP} + \varphi_S + \left[\frac{1}{C_{OX}} + \frac{1}{C_{FN}\ (\alpha = 0)} \right] \cdot \int_0^{\varphi_S} C_S d\varphi_S \tag{12}$$

$$V_{G,RCP-TRG} = V_{FB,RCP-TRG} + \varphi_S + \left[\frac{1}{C_{OX}} + \frac{1}{C_{FN}\ (\alpha > 0)} \right] \cdot \int_0^{\varphi_S} C_S d\varphi_S \tag{13}$$

Because S_V is calculated at a fixed I_D or the same φ_S after receptor immobilization and after receptor–target binding, the expression for S_V in (3) is rewritten by subtracting (13) from (12) as follows:

$$S_V = V_{FB,RCP} - V_{FB,RCP-TRG} + \left[\frac{1}{C_{FN}\ (\alpha = 0)} - \frac{1}{C_{FN}\ (\alpha > 0)} \right] \cdot \int_0^{\varphi_S} C_S d\varphi_S \tag{14}$$

Let the effective overall capacitance of the functionalization layer, $C_{FN,EFF}$, be

$$C_{FN,EFF} = \left[\frac{1}{C_{FN}\ (\alpha = 0)} - \frac{1}{C_{FN}\ (\alpha > 0)} \right]^{-1} \tag{15}$$

Then, using (9) and considering $A_{CH}/A_{GT} = \sim 10^{-3}$ for the fabricated device,

$$C_{FN,EFF} = \left[\frac{A_{CH}}{A_{GT}} \cdot \frac{1}{\left(\frac{1}{\alpha} - 1\right) \cdot C_{RCP,CH} + \frac{1}{\alpha} \cdot C_{TRG,CH}} + \frac{1}{\left(\frac{1}{\alpha} - 1\right) \cdot C_{RCP,CH} + \frac{1}{\alpha} \cdot C_{TRG,CH}} \right]^{-1} \cong \left(\frac{1}{\alpha} - 1\right) \cdot C_{RCP,CH} + \frac{1}{\alpha} \cdot C_{TRG,CH} \tag{16}$$

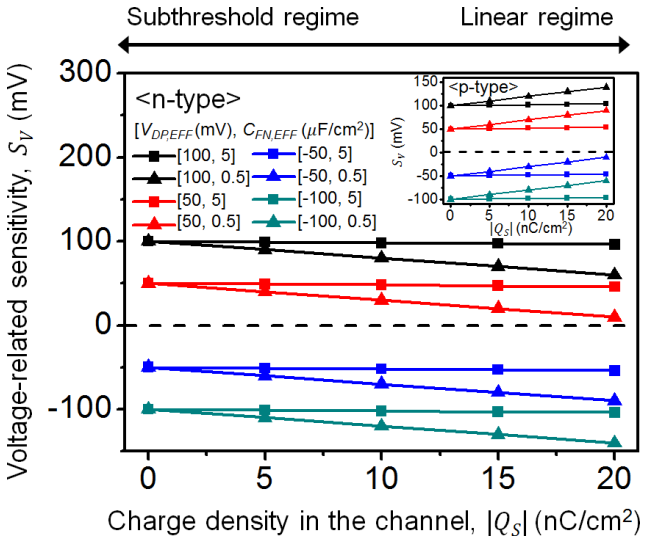

FIGURE 5. Calculated S_V dependency with varying Q_S related to operation regime for an n-type EGT, where $V_{DP,EFF} = -100$, -50, 50, and 100 mV and $C_{FN,EFF} = 0.5$ and 5 μF/cm^2. Inset: S_V vs. Q_S for a p-type EGT.

Fig. 4 shows the $C_{FN,EFF}$ variation as a function of α with $C_{RCP,CH} = 0.5$, 5 μF/cm^2 and $C_{TRG,CH} = 0.5$, 5 μF/cm^2, respectively. The $C_{FN,EFF}$ values are strongly dependent on α, and at least one order of magnitude of $C_{FN,EFF}$ is changed for $0.05 < \alpha < 1$. In addition, a lower $C_{TRG,CH}$ with a higher $C_{RCP,CH}$ generates more variation in $C_{FN,EFF}$, as shown in Fig. 4.

Using (4), $C_{FN,EFF}$ can be calculated as follows:

$$C_{FN,EFF} = C_{TRG,CH} + (C_{TRG,CH} + C_{RCP,CH}) \frac{K}{[TRG]^n} \quad (17)$$

Finally, S_V can be expressed as follows:

$$S_V = V_{DP,EFF} + \frac{Q_S}{C_{FN,EFF}} \quad (18)$$

Thus, the values of $V_{DP,EFF}$, $C_{FN,EFF}$, and Q_S affect the sensitivity. Fig. 5 shows the S_V dependence on the operation regime with different $V_{DP,EFF}$, $C_{FN,EFF}$ values in an n-type EGT using (18). The polarity of $V_{DP,EFF}$ determines the direction of the shift in the transfer curve after the binding event. For an n-type EGT ($Q_S < 0$), a positive $V_{DP,EFF}$ decreases V_{FB} and V_{TH}, causing the I_D–V_G curve to shift toward a negative V_G direction, followed by a positive S_V. Lower values of $C_{FN,EFF}$ lead to a decrease in S_V because of the negative Q_S. In addition, the subthreshold regime ($V_G < V_{TH}$) provides a higher S_V compared with the linear regime ($V_G > V_{TH}$) owing to a smaller Q_S. In contrast, negative values of $V_{DP,EFF}$ provide a higher absolute sensitivity with a smaller $C_{FN,EFF}$ in the linear regime.

B. PA DETECTION WITH SENSITIVITY ANALYSIS

Peanut allergen (PA) detection was conducted using the fabricated n-type SiNN EGT to evaluate the S_V characteristics relevant to $V_{DP,EFF}$ and $C_{FN,EFF}$. Fig. 6(a) shows representative

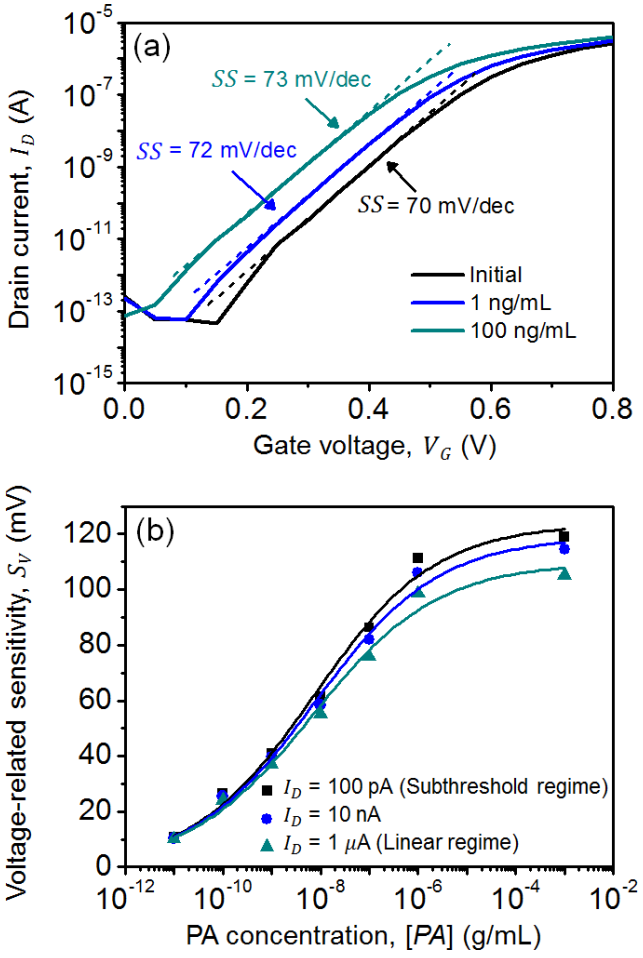

FIGURE 6. (a) Representative transfer curves of the SiNN EGTs with [PA], (b) average S_V with various I_D and [PA]. The solid lines are fitted lines of S_V vs. [PA] with a range of 10 pg/mL–1 mg/mL PA (black: I_D = 100 pA, blue: I_D = 10 nA, cyan: I_D = 1 μA).

transfer curves of the device with different PA concentrations ([PA]). Initially, the device shows a typical n-type FET behavior and has excellent electrical characteristics including a low V_{TH} of ~0.58 V, a low SS of ~70 mV/dec, a low gate leakage current of <10 pA, and a high on/off current ratio of ~10^7. When the device was exposed to PA, the curve shifted toward the negative V_G direction, and a degradation of SS was observed. The degradation of SS is mainly caused by the change in C_{FN} due to receptor–target binding [25]:

$$SS = \left[\frac{d\,(\log_{10} I_D)}{dV_G}\right]^{-1} = \frac{2.3kT}{q}\left[1 + C_D\left(\frac{1}{C_{OX}} + \frac{1}{C_{FN}}\right)\right] \quad (19)$$

where kT/q is the thermal voltage, and C_D is the depletion capacitance. As SS increases, a larger V_G is required to achieve the same I_D value. From (9) and (19), a higher α causes a decrease in C_{FN}, followed by a degradation of SS.

Fig. 6(b) shows the extracted S_V as a function of [PA] with different I_D values. The fitted curve is a logistic equation

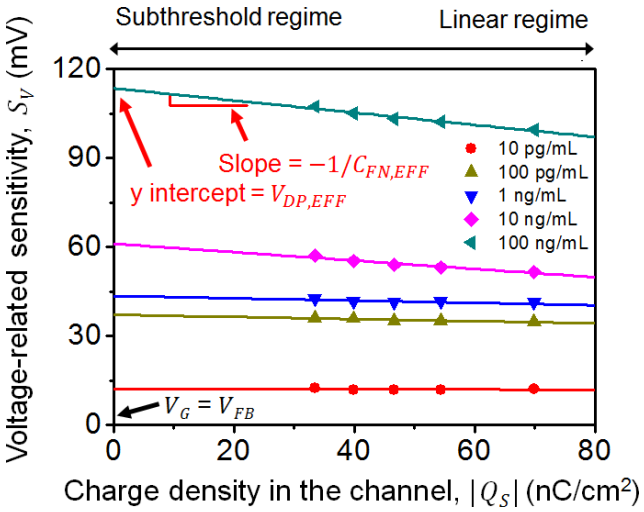

FIGURE 7. Representative graph of $|Q_S|$ vs. S_V depending on [*PA*]. Solid lines are fitted lines of $|Q_S|$ vs. S_V at each [*PA*].

that is widely applied at a nonlinear relationship between the output response and analyte concentration [22], [23], [26]. The dynamic range of the device was more than four orders of magnitude in the range of 100 pg/mL to 1 μg/mL. The operation in the subthreshold regime provides a slightly higher S_V compared to that in the linear regime. For example, 10% of S_V was enhanced at 1 mg/mL PA as I_D decreased from 1 μA (linear regime) to 100 pA (subthreshold regime).

Fig. 7 shows the S_V versus Q_S characteristics for different [*PA*] values. Q_S is calculated using (1) and (2). The positive values of $V_{DP,EFF}$ are obtained from the y-intercept and are clearly proportional to [*PA*] according to (18). A higher S_V in the subthreshold regime matches well with the case of $V_{DP,EFF} > 0$. The extracted $C_{FN,EFF}$ values from the reciprocal of the slope are independent of V_G and are affected only by [*PA*].

Fig. 8 shows the extracted $V_{DP,EFF}$ and $C_{FN,EFF}$ as a function of the logarithm of [*PA*]. The logistic calibration curve of $V_{DP,EFF}$ was obtained as $V_{DP,EFF} = 143.82 \times [PA]^{0.35}/(1.84 \times 10^{-3} + [PA]^{0.35})$. Then, using (4) and (5), α can be calculated as $\alpha = [PA]^{0.35}/(1.84 \times 10^{-3} + [PA]^{0.35})$ with $K = 1.84 \times 10^{-3}$ and $n = 0.35$, where $n < 1$ indicates a negative cooperativity of the PA binding. The increase in $V_{DP,EFF}$ for higher [PA] is due to the increase in α.

$C_{FN,EFF}$ with the extracted K and n values is fitted as $C_{FN,EFF} = 2.5 \times 10^{-6} + 1.13 \times 10^{-8} \times [PA]^{-0.35}$ using (17). The extracted $C_{TRG,CH}$ and $C_{RCP,CH}$ values are 2.5 μF/cm^2 and 3.65 μF/cm^2, respectively. A higher *PA* increases the binding factor α, followed by a decrease in $C_{FN,EFF}$.

Fig. 9 shows the variation in S_V, $V_{DP,EFF}$, and $Q_S/C_{FN,EFF}$ with different [*PA*] values. In the PA detection, the sum of the positive $V_{DP,EFF}$ and negative $Q_S/C_{FN,EFF}$ produces the overall S_V in n-type EGTs. The influence of $Q_S/C_{FN,EFF}$ on S_V becomes profound as [*PA*] increases and/or the device is operated in the linear regime.

The LOD is another critical parameter for detecting a specific biomolecule. The 3-sigma method has been widely

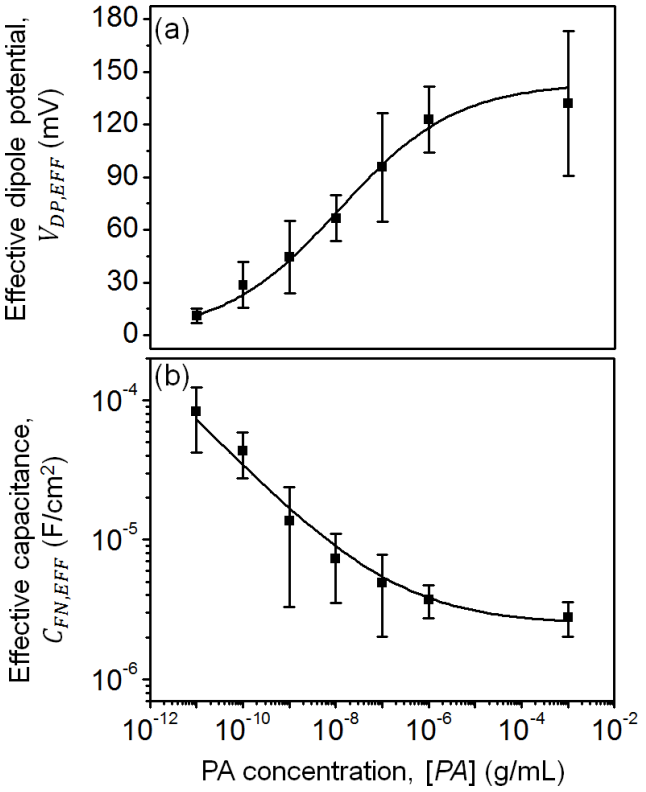

FIGURE 8. (a) $V_{DP,EFF}$ and (b) $C_{FN,EFF}$ for various [*PA*], which are extracted from Fig. 7. The solid lines are fitted lines in an x-axis range of 10 pg/mL–1 mg/mL of [*PA*].

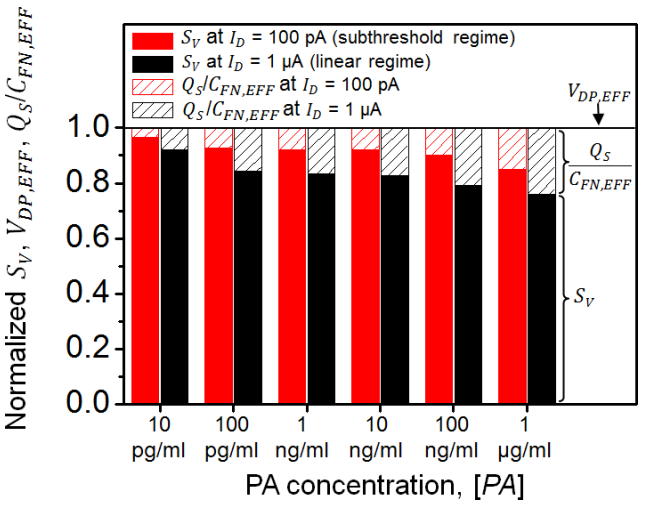

FIGURE 9. Normalized S_V, $V_{DP,EFF}$, and $Q_S/C_{FN,EFF}$ divided by $V_{DP,EFF}$ depending on operation regimes for various [*PA*] values.

applied to calculate the LOD, which is the extracted [*PA*] at which the S_V is equal to three times the standard deviation of S_V in a blank sample without PA [27], [28]. Fig. 10 shows the calculated LODs for different operation regimes. LODs were calculated to be as low as 70, 90, and 130 pg/mL for $I_D = 100$ pA, 10 nA, and 1 μA, respectively. The LOD in the

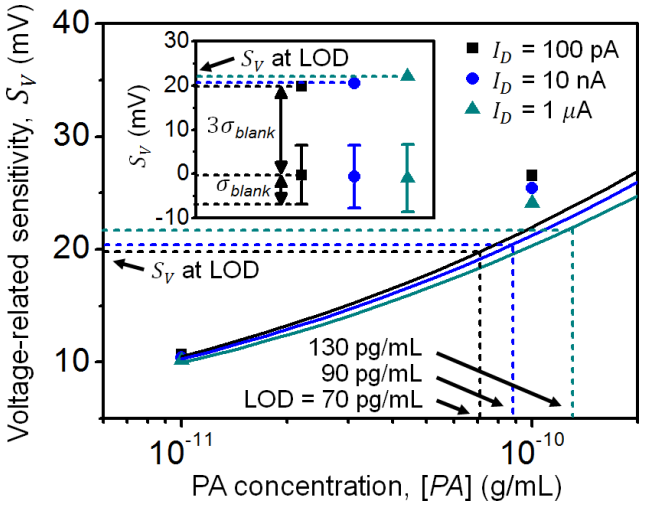

FIGURE 10. LOD extraction with the 3-sigma method at various operation regimes. The solid line is a fitted line of S_V vs. [PA]. Inset: lower points with error bars are the S_V values of blank replicates with different regimes, and the upper points are the S_V values calculated from the 3-sigma method.

subthreshold regime ($I_D = 100$ pA) was ~2 times lower than that in the linear regime ($I_D = 1$ μA).

IV. CONCLUSION

We presented the influence of receptors and targets on sensing characteristics using analytical modeling and verified this model by detecting peanut allergens with SiNN EGTs. Using a lumped capacitor model, the dipole moment $V_{DP,EFF}$ and the capacitance $C_{FN,EFF}$ due to the receptor–target binding on the surface of the device and the operation regime were found to be crucial to achieving high sensing performance. When $V_{DP,EFF} > 0$, the operation in the subthreshold regime can provide a better sensitivity, which is enhanced as the $C_{FN,EFF}$ values increase. When $V_{DP,EFF} < 0$, the device needs to be operated in the linear regime for higher sensitivity with smaller $C_{FN,EFF}$ values. From the experimental results of PA detection, $V_{DP,EFF}$, $C_{FN,EFF}$ were successfully extracted as a function of the PA concentration. The PA sensitivity with $V_{DP,EFF} > 0$ was higher in the subthreshold regime ($V_G < V_{TH}$) than in the linear regime ($V_G > V_{TH}$). In addition, the lowest LOD of 70 pg/mL is achieved in the subthreshold regime. These results confirm that the proposed model is utilized to optimize the sensing characteristics of Si-based EGT for numerous applications in highly sensitive, highly reliable, and disposable biosensors.

REFERENCES

[1] Y. Cui, Q. Wei, H. Park, and C. M. Lieber, "Nanowire nanosensors for highly sensitive and selective detection of biological and chemical species," *Science*, vol. 293, no. 5533, pp. 1289–1292, Aug. 2001.
[2] B. Ding, M. Wang, X. Wang, J. Yu, and G. Sun, "Electrospun nanomaterials for ultrasensitive sensors," *Mater. Today*, vol. 13, no. 11, pp. 16–27, Nov. 2010.
[3] F. Patolsky, G. Zheng, and C. M. Lieber, "Fabrication of silicon nanowire devices for ultrasensitive, label-free, real-time detection of biological and chemical species," *Nature Protocols*, vol. 1, no. 4, pp. 1711–1724, Nov. 2006.
[4] O. Knopfmacher, A. Tarasov, W. Fu, M. Wipf, B. Niesen, M. Calame, and C. Schönenberger, "Nernst limit in dual-gated Si-nanowire FET sensors," *Nano Lett.*, vol. 10, pp. 2268–2274, Jun. 2010.
[5] A. Gao, N. Lu, P. Dai, T. Li, H. Pei, X. Gao, Y. Gong, Y. Wang, and C. Fan, "Silicon-nanowire-based CMOS-compatible field-effect transistor nanosensors for ultrasensitive electrical detection of nucleic acids," *Nano Lett.*, vol. 11, no. 9, pp. 3974–3978, Sep. 2011.
[6] Y. Kanai, Y. Ohmuro-Matsuyama, M. Tanioku, S. Ushiba, T. Ono, K. Inoue, T. Kitaguchi, M. Kimura, H. Ueda, and K. Matsumoto, "Graphene field effect transistor-based immunosensor for ultrasensitive noncompetitive detection of small antigens," *ACS Sensors*, vol. 5, no. 1, pp. 24–28, Jan. 2020.
[7] S. Li, K. Huang, Q. Fan, S. Yang, T. Shen, T. Mei, J. Wang, X. Wang, G. Chang, and J. Li, "Highly sensitive solution-gated graphene transistors for label-free DNA detection," *Biosens. Bioelectron.*, vol. 136, pp. 91–96, Jul. 2019.
[8] S. Hideshima, R. Sato, S. Inoue, S. Kuroiwa, and T. Osaka, "Detection of tumor marker in blood serum using antibody-modified field effect transistor with optimized BSA blocking," *Sens. Actuators B, Chem.*, vol. 161, no. 1, pp. 146–150, Jan. 2012.
[9] K. Guo, S. Wustoni, A. Koklu, E. Díaz-Galicia, M. Moser, A. Hama, A. A. Alqahtani, A. N. Ahmad, F. S. Alhamlan, M. Shuaib, A. Pain, I. McCulloch, S. T. Arold, R. Grünberg, and S. Inal, "Rapid single-molecule detection of COVID-19 and MERS antigens via nanobody-functionalized organic electrochemical transistors," *Nature Biomed. Eng.*, vol. 5, no. 7, pp. 666–677, Jul. 2021.
[10] N. Elfström, R. Juhasz, I. Sychugov, T. Engfeldt, A. E. Karlström, and J. Linnros, "Surface charge sensitivtity of silicon nanowires: Size dependence," *Nano Lett.*, vol. 7, no. 9, pp. 2608–2612, Sep. 2007.
[11] M. M. N. Nuzaiha, U. Hashim, M. K. Md Arshad, S. R. Kasjoo, S. F. A. Rahman, A. R. Ruslinda, M. F. M. Fathil, R. Adzhri, and M. M. Shahimin, "Electrical detection of dengue virus (DENV) DNA oligomer using silicon nanowire biosensor with novel molecular gate control," *Biosens. Bioelectron.*, vol. 83, pp. 106–114, Sep. 2016.
[12] T. T. K. Nguyen, T. N. Nguyen, G. Anquetin, S. Reisberg, V. Noël, G. Mattana, J. Touzeau, F. Barbault, M. C. Pham, and B. Piro, "Triggering the electrolyte-gated organic field-effect transistor output characteristics through gate functionalization using diazonium chemistry: Application to biodetection of 2,4-dichlorophenoxyacetic acid," *Biosens. Bioelectron.*, vol. 113, pp. 32–38, Aug. 2018.
[13] M. Y. Mulla, E. Tuccori, M. Magliulo, G. Lattanzi, G. Palazzo, K. Persaud, and L. Torsi, "Capacitance-modulated transistor detects odorant binding protein chiral interactions," *Nature Commun.*, vol. 6, p. 6010, Jan. 2015.
[14] E. Macchia, K. Manoli, B. Holzer, C. D. Franco, M. Ghittorelli, F. Torricelli, D. Alberga, G. F. Mangiatordi, G. Palazzo, G. Scamarcio, and L. Torsi, "Single-molecule detection with a millimetre-sized transistor," *Nature Commun.*, vol. 9, no. 1, p. 3223, Aug. 2018.
[15] P. Lin, X. Luo, I.-M. Hsing, and F. Yan, "Organic electrochemical transistors integrated in flexible microfluidic systems and used for label-free DNA sensing," *Adv. Mater.*, vol. 23, no. 35, pp. 4035–4040, Sep. 2011.
[16] H. Sirringhaus, "Reliability of organic field-effect transistors," *Adv. Mater.*, vol. 21, nos. 38–39, pp. 3859–3873, Oct. 2009.
[17] P. A. Bobbert, A. Sharama, S. G. J. Mathijssen, M. Kemerink, and D. M. de Leeuw, "Operational stability of organic field-effect transistors," *Adv. Mater.*, vol. 24, pp. 1146–1158, Mar. 2012.
[18] Y. Zhang, Z. Wu, K. Li, X. Li, A. Yang, P. Tong, and H. Chen, "Allergenicity assessment on thermally processed peanut influenced by extraction and assessment methods," *Food Chem.*, vol. 281, pp. 130–139, May 2019.
[19] J. He, F. Liu, W. Bian, J. Feng, J. Zhang, and X. Zhang, "An approximate carrier-based compact model for fully depleted surrounding-gate MOSFETs with a finite doping body," *Semicond. Sci. Technol.*, vol. 22, no. 6, pp. 671–677, May 2007.
[20] S. Lee, "Bias-dependent subthreshold characteristics and interface states in disordered semiconductor thin-film transistors," *Semicond. Sci. Technol.*, vol. 34, no. 11, Oct. 2019, Art. no. 11LT01.
[21] K. Shoorideh and C. O. Chui, "Optimization of the sensitivity of FET-based biosensors via biasing and surface charge engineering," *IEEE Trans. Electron Devices*, vol. 59, no. 11, pp. 3104–3110, Nov. 2012.
[22] N. Tajima, M. Takai, and K. Ishihara, "Significance of antibody orientation unraveled: Well-oriented antibodies recorded high binding affinity," *Anal. Chem.*, vol. 83, no. 6, pp. 1969–1976, Feb. 2011.
[23] B. I. Kurganov, A. V. Lobanov, I. A. Borisov, and A. N. Reshetilov, "Criterion for Hill equation validity for description of biosensor calibration curves," *Analytica Chim. Acta*, vol. 427, no. 1, pp. 11–19, Jan. 2001.

[24] P. Georgiou and C. Toumazou, "ISFET characteristics in CMOS and their application to weak inversion operation," *Sens. Actuators B, Chem.*, vol. 143, no. 1, pp. 211–217, 2009.
[25] Y. Taur and T. H. Ning, "MOSFET devices," in *Fundamentals of Modern VLSI Devices*, 2nd ed. Cambridge, U.K.: Cambridge Univ. Press, 2009, ch. 2, pp. 148–203.
[26] J. Tschmelak, M. Kumpf, N. Kappel, G. Proll, and G. Gauglitz, "Total internal reflectance fluorescence (TIRF) biosensor for environmental monitoring of testosterone with commercially available immunochemistry: Antibody characterization, assay development and real sample measurements," *Talanta*, vol. 69, no. 2, pp. 343–350, Apr. 2006.
[27] A. Gao, N. Lu, Y. Wang, and T. Li, "Robust ultrasensitive tunneling-FET biosensor for point-of-care diagnostics," *Sci. Rep.*, vol. 6, Mar. 2016, Art. no. 22554.
[28] A. Shrivastava and V. B. Gupta, "Methods for the determination of limit of detection and limit of quantitation of the analytical methods," *Chronicles Young Scientists*, vol. 2, no. 1, pp. 21–25, Apr. 2011.

DONGHOON KIM received the B.S. degree in electrical engineering from the Pohang University of Science and Technology (POSTECH), South Korea, in 2014, and the M.S. degree in electrical engineering from the Jeong-Soo Lee's Group, POSTECH, in 2016, where he is currently pursuing the Ph.D. degree. His research interests include nanoscaled electronic devices and bio/chemical-sensor applications.

WONYEONG CHOI received the B.S. degree from the Department of Electrical Engineering, Pohang University of Science and Technology (POSTECH), South Korea, in 2016, and the M.S. degree in electrical engineering from the Jeong-Soo Lee's Group, POSTECH, in 2018, where he is currently pursuing the Ph.D. degree. His research interests include nanoscaled electronic devices, and the bio sensor applications.

SEONGHWAN SHIN received the B.S. degree from the Department of Electronics Engineering, Kyungpook National University, South Korea, in 2018, and the M.S. degree in electrical engineering from the Jeong-Soo Lee's Group, POSTECH, in 2021, where he is currently pursuing the Ph.D. degree. He is focusing on nanoscaled electronic devices, and the bio sensor applications.

JIWON PARK received the B.S. degree from the Department of Electrical Engineering, Pohang University of Science and Technology (POSTECH), South Korea, in 2020, where he is currently pursuing the M.S. degree in electrical engineering with the Jeong-Soo Lee's Group. He is focusing on nanoscaled electronic devices, and the bio sensor applications.

KIHYUN KIM (Member, IEEE) received the B.S. degree in electrical engineering from Hanyang University, in 2009, and the Ph.D. degree in electrical engineering from the Pohang University of Science and Technology (POSTECH), Pohang, South Korea, in 2015. He was a Senior Researcher with the Future IT Innovation Laboratory, POSTECH, from 2015 to 2017. He was a Research Assistant Professor with the Department of Creative IT Engineering, POSTECH, from 2017 to 2019. He was a Visiting Scholar at the NASA Ames Research Center, in 2019, where he developed gas sensor and infrared photodetector. Since 2019, he has been an Assistant Professor with the Division of Electronic Engineering, Jeonbuk National University. His research interests include advanced Si nanodevice fabrication and applications, such as silicon nanowire-based chemical and biological sensors, near infrared photodetector, and thermoelectric devices.

BO JIN received the B.S. degree in electrical communication engineering from Yanbian University of Science and Technology (YUST), Yanji, China, in 2009, and the Ph.D. degree in IT convergence engineering from Pohang University of Science and Technology (POSTECH), Pohang, Republic of Korea, in 2015. He worked as a research assistant professor in electrical engineering in POSTECH since 2015. Also since 2016, he joined Innovative General Electronic Sensor Technology co., ltd. (IGEST) in Republic of Korea, and worked as a Technical director. His current research interests include power device, nanoscale materials & devices, and biosensor & chemical sensor applications.

JEONG-SOO LEE (Senior Member, IEEE) received the B.S., M.S., and the Ph.D. degrees in electrical engineering from POSTECH, South Korea, in 1991, 1993, and 1996, respectively. In 1996, he joined Samsung Electronics and worked as a Senior Engineer on the development of logic devices and nonvolatile memory devices. He was a Visiting Scholar at UC Berkeley, in 2001, where he developed Fin-FETs and ultra-thin-body (UTB) FETs. In 2005, he was a Founding Member of the National Center of Nanomaterials Technology (NCNT) established by the Ministry of Knowledge Economy, South Korea. Since 2008, he has been a Full Professor with the Department of Electrical Engineering, POSTECH, and also worked as the Vice-Director at the NCNT. His research interests include Si-based nonplanar transistors, nanoscale CMOS devices, bottom-up nanowire transistors, and their biosensor applications.